

Enhanced Visible Light Photocatalytic Activity of Lead Selenide/Graphene/Titanium Dioxide Nanocomposite Synthesized *via* Ultra-Sonication Technique

ASGHAR ALI and WON-CHUN OH*

Department of Advanced Materials Science & Engineering, Hanseo University, Seosan 31962, Republic of Korea

*Corresponding author: Fax: +82 41 6883352; Tel: +82 41 6601337; E-mail: wc_oh@hanseo.ac.kr

Received: 23 June 2017;

Accepted: 22 September 2017;

Published online: 30 November 2017;

AJC-18644

In this study, we investigated the photo-degradation efficiency of PbSe-G-TiO₂ ternary nanocomposite under visible light irradiation using rhodamine B as standard dye. A nanocomposite was synthesized by ultra-sonication technique and characterized by X-ray diffraction, scanning electron microscopy, transmission electron microscopy, Raman spectroscopic analysis and UV-visible absorbance spectra analysis. The results indicate that PbSe-G-TiO₂ ternary nanocomposite has excellent stability and good photodegradation efficiency than PbSe-G and TiO₂-G nanocomposite which is approximately 92.5 % of rhodamine B degradation after visible light irradiation for 180 min.

Keywords: Graphene, Photocatalytic activity, Nanocomposite, PbSe-G-TiO₂, Rhodamine B dye.

INTRODUCTION

Textile industries are major cause of an environmental population, not only utilize large amount of water but also produce enormous volume of wastewater during the dyeing processes [1]. It consists of highly intense colored and other contaminated substance and these wastewater are not ignorable, because its direct or indirect effected to human as well as aquatic life. Therefore, textile dyeing wastewater treatment has received more attention in the last few decades [2-4]. Different techniques are used for removing hydrophobic dyes, such as electron oxidation, ozonation, electro-kinetic coagulation ion, membrane filtration and microbial degradation [5-10]. These techniques have some advantages and disadvantages over the other techniques. Therefore suitable techniques are required to use to degrade the dye form water. among of these techniques heterogeneous photocatalysis by semiconductors materials as favourable techniques and been extensively used for the removal of toxic dyes, due to their well-defined electrochemistry, excellent redox recyclability and outstanding environmental stability, therefore researcher choose photocatalytic degradation technique to eliminate dyes form wastewater [11-14]. Recently TiO₂ has been used for the photo-degradation due to their exclusive properties, such as excellent chemical stability, nontoxicity, inexpensive and high photocatalytic efficiency [15]. However, the uses of TiO₂ still limit due to its high energy band gap (3.2 eV) and fast recombination of electron hole pair, the photo generated electron and holes in the excited states are unstable and promptly recombine, dissipating the input

energy as heat resulting minimize photocatalytic efficiency [16-18]. Therefore to increase the efficiency of TiO₂ some modification are carried out, *i.e.* doping TiO₂ with metal [19,20] and non-metal [21,22] or coupling TiO₂ with narrow band gap semiconductors [23,24] and coupling with carbon nano material *i.e.* graphene [25]. Graphene flat monolayer structure and widely investigated for its intriguing electrical and mechanical properties [26-28]. Furthermore graphene great ability by anchoring nanoparticles, *i.e.* PbSe and improve their photocatalytic efficiency and overcome recombination process. Many synthesis techniques such as hydrothermal, microwave and sol-gel have been developed to attachment of nanoparticles on the graphene sheets [29,30]. In present work, we prepare PbSe-G-TiO₂ photocatalyst by an ultra-sonication technique. The prepared samples are used for photo-degradation. The photo catalytic activities were tested with rhodamine B as a standard dye under visible light irradiation.

EXPERIMENTAL

Graphene oxide prepared from pure graphite in the laboratory by the Hummers-Offeman method [31,32]. Selenium powder (99 %), ammonium hydroxide (25-28 %) and titanium *n*-butoxide (TNB, C₁₆H₃₆O₄Ti) were purchased from Samchun Pure Chemical. Sodium sulfite and ethyl alcohol (94 %) were purchased from Duksan Pure Chemical Co. Ltd. Lead chloride and ammonium hydroxide (28 %) was purchased from Junsci Chemical Co. Ltd., Korea. All chemicals were used without further purification and all dilutions were carried out using distilled water.

Synthesis of lead selenide: PbSe was synthesized through ultra-sonic technique, in synthesis procedure; 1.5 g of anhydrous sodium sulfite and 0.20 g of crude selenium powder were continuously stirred with 150 mL of ethylene glycol providing constant temperature of 70 °C to form Na_2SeSO_3 . After that 1 mL of both Na_2SeSO_3 and PbCl_2 were mixed and solution were ultrasonicated using a digital sonifer for 2 h at 90 °C. Finally, PbSe precipitates were obtained using 47 mm Whatman filter paper. The residue was washed off with distilled water, at least five times. The collected PbSe powder was dried in vacuum oven at a temperature of 80 °C for 10 h.

Synthesis of binary PbSe-G and ternary PbSe-G-TiO₂ composites: In this process, PbSe particles and 200 mg of graphene oxide (previously obtained by the Hummers-Offeman method) with a ratio of 1:1 (wt:wt) were dissolved in 150 mL of ethylene glycol. Then the solution was ultrasonicated for 2 h at 80 °C. After ultra-sonication the graphene oxide was reduced to graphene nanosheet and PbSe compounds were grown on the graphene surface. The solution was filter with 47 mm Whatman filter paper with a pore size of 0.7 mm and then cool and settle at room temperature. The resultant powder was washed with distilled water 3 times, followed by drying in the vacuum oven. The powder was heated to 100 °C for 8 h in vacuum oven, to complete the formation of PbSe-G composite nanostructures. Same procedure was followed for the syntheses of ternary PbSe-G-TiO₂. Different concentration TNB was mixed to the PbSe-G and the solution was sonicated at room temperature for 3 h using a controllable serial-ultrasonic apparatus (Ultrasonic Processor, VCX 750, Korea). The final product was heat treated at 500 °C for 2 h in an electric furnace. The prepared sample was labeled PbSe-G-TiO₂.

Photocatalytic degradation experiment of rhodamine B: The adsorption and photocatalytic performance of the as-prepared PbSe-G-TiO₂ was investigated by the degradation of rhodamine B dye under visible light. First 30 mg of PbSe-G-TiO₂ catalytic sample was put on 100 mL solution of rhodamine B (2.5×10^{-6} mol/L). In order to reach adsorption-desorption equilibrium, the solution was kept in dark for 2 h. Then 10 mL sample was collected from the solution and kept in a centrifuge at 10,000 rpm for the elimination of solid materials. After that, the light source was turn on. The samples were collected in every 30 min and then centrifuged for 10 min to remove any suspended solid. All the samples were irradiated for 180 min to compare their catalytic efficiencies.

Characterization: X-ray diffraction (Shimadzu XD-D1, Uki, Kumamoto, Japan) was used to describe the crystallinity of the composite with monochromatic high-intensity $\text{CuK}\alpha$ radiation ($\lambda = 1.5406 \text{ \AA}$). SEM (JSM-5600, JEOL Ltd., Tokyo, Japan) was used to examine the surface morphology of the PbSe-G-TiO₂ nanocomposite. Transmission electron microscopy (TEM, JEOL, JEM-2010, Japan) was used to explain the state and particle size of the prepared composite and Raman spectra of the prepared samples were observed using a spectrometer (Jasco Model Name NRS-3100) with an excitation laser wavelength of 532.06 nm. The photocatalytic performance of the prepared samples was investigated by absorbance spectrometry with a UV/visible spectrophotometer (Optizen POP, Mecasys, Korea).

RESULTS AND DISCUSSION

Phase structure of prepared nanocomposite was examined by XRD technique. Fig. 1 displays the XRD pattern of PbSe-G-TiO₂, which exhibit that the diffraction peaks of the PbSe-G around 2θ of 29.60, 43.00, 48.50, 53.00, 60.80, 76.00, 69.00 and 77.70°, which can be indexed to the characteristic plane reflections (200), (220), (311), (222), (400), (331), (420) and (442) reflection that correspond to the clausthalite crystal phase (JCPDS PDF# 00-065-0327) [33]. While TiO₂ are $2\theta = 26.30, 37.94, 54.56$ and 80.88 corresponding to the (111), (004), (105) and (224) diffractions as anatase crystal phase (JCPDS PDF#00-021-1272) [34]. After the attachment of PbSe on the graphene nanosheet a small intensity peaks at $2\theta = 26.2^\circ$, which corresponds to the (002) diffraction peak of graphene. This observation verify that PbSe nanocomposite was successfully synthesized and attached on graphene sheet [35].

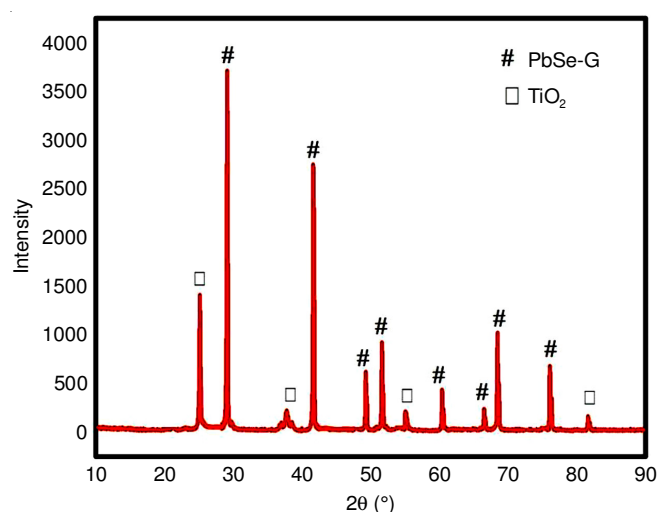


Fig. 1. X-ray diffraction patterns of PbSe-G-TiO₂ composites

Fig. 2(a-c) show the morphology of the PbSe-G-TiO₂ nanocomposites. The SEM illustrates the overall surface morphology of graphene composites, Fig. 2(a) express that graphene sheet have a flaky texture broken off in different direction and PbSe nanocomposites unevenly distributed on graphene sheet and the graphene sheet acts as bridge for PbSe nanoparticles, which helpful to provide a path for the photo-generated electron and increase photo catalytic efficiency [36]. Fig. 2(b) shows that the TiO₂ particles are roughly distributed on graphene sheet and large interlayer spaces and thin layer edges of graphene can be clearly observed. Fig. 2(c) displays the PbSe-G-TiO₂ nanocomposites. From the images clearly shows the difference between binary and ternary composites. After attachment of TiO₂, the brighter spot arises in the ternary composite suggesting that uniformly dispersed on graphene nanosheet. TEM images of a PbSe-G-TiO₂ nanocomposite with different magnification (200 nm to 1 μm) were displayed in the Fig. 3(a-b), which demonstrated the overall history of the PbSe and TiO₂ nanoparticles. From the Fig. 3, it is clearly seen that PbSe and TiO₂ nanoparticles were spherical from and uniformly distributed on the graphene sheet, the average size of PbSe and TiO₂ to be approximately 6-25 and 9-18 nm, respectively. The particle further confirms the uniform distri-

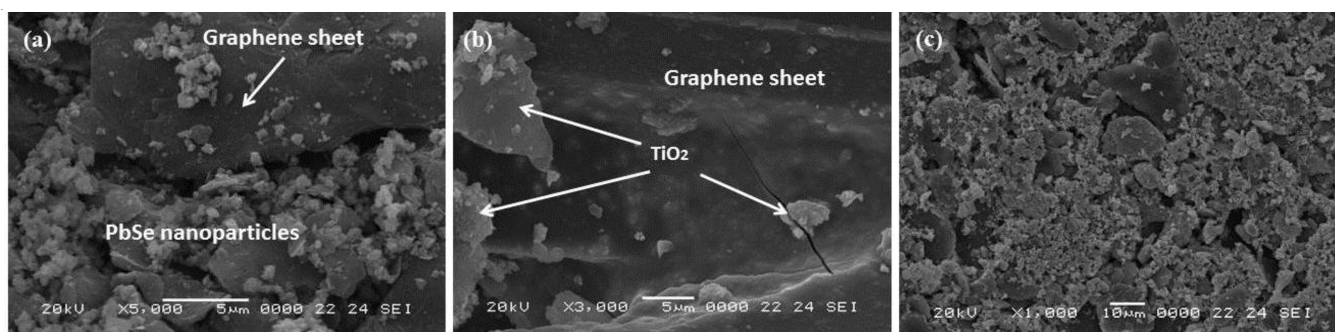


Fig. 2. SEM images of PbSe-G, TiO₂-G and PbSe-G-TiO₂ composites

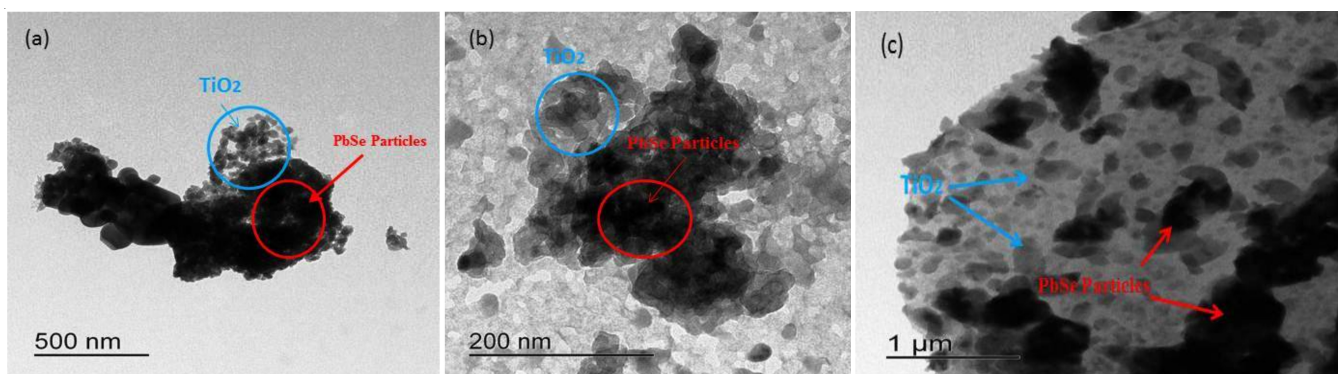


Fig. 3. TEM images of PbSe-G-TiO₂ composites with different magnification

bution and strong heterojunction of PbSe and TiO₂. A spherical and uniform particle size of PbSe further confirm that the presence of GO inhibits the growth of PbSe crystals due to the electrostatic attraction between Pb²⁺ and negatively charged GO [37] at initial reaction stage, Pb²⁺ is reduced to Pb and PbSe forms by the reaction Pb⁺, Se⁻ [37].

Raman spectroscopy is a highly advance technique to study the structural information of carbon-based materials [38]. The PbSe-G-TiO₂ was further characterized by Raman scattering spectroscopy techniques. Fig. 4 shows the peaks related to anatase TiO₂ are observed in 510-410 cm⁻¹ region [39-41]. The characteristic graphitic peaks, D and G peak of GO are appear at 1375 and 1585 cm⁻¹ respectively. The G band appears at the first order scattering of the optical E_{2g} Phonon of sp² carbon

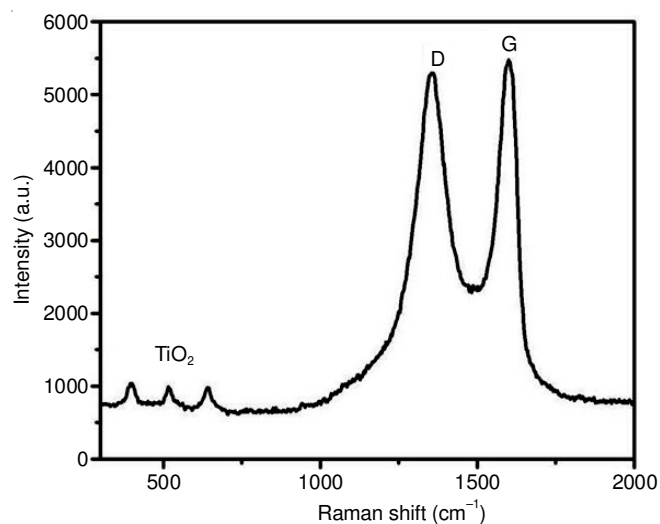


Fig. 4. Raman spectra of PbSe-G-TiO₂ nanocomposite

atoms and D band comes from A_{1g} symmetry [42]. These two bands (D 1360 cm⁻¹, G 1590 cm⁻¹) indicate an interaction between GO and selenide nanosheets, the nature of the defects can find the ratio intensities of D and G band, the ratio intensities of G and D band approximately 0.965, which is smaller than graphene oxide. The decreasing ratio is clear evidence of the increased number of graphene layers.

The photocatalytic activities of PbSe-G-TiO₂ nanocomposite using rhodamine B as organic dye under visible irradiation was explored Fig. 5(a-c). Which shows decreasing intensity of electronic absorption spectra (λ_{\max}) with different interval of time, exhibited that the degradation of rhodamine B in the presence of PbSe-G-TiO₂ catalysts. The λ_{\max} value of PbSe-G-TiO₂ was found to 555 nm and PbSe-G-TiO₂ ternary nano composite intensity decreased approximately 92.2 % at the end of 180 min the excellent efficiency attributed due to the three factors: (a) good absorption by PbSe-G-TiO₂ photocatalyst, (b) fast charge transfer route and (c) graphene acts an adsorption support material and dye absorbs molecules on the surface of graphene *via* π - π interaction, Fig. 5(a) demonstrates that the concentration of rhodamine B change due to the different interval of time, which shows the good absorption efficiency of rhodamine B of PbSe-G-TiO₂ nanocomposites. For achieving adsorption-desorption equilibrium, the prepared sample was kept in dark for 30 min, after obtain the adsorption-desorption equilibrium, the solution was kept in closed box and turn on visible light. The solution was irradiated for 30 min and every 30 min sample was taken out from the chamber for further syntheses. Then the sample was centrifuge and find dye concentration using UV-visible spectrometer. The photo catalytic performance of different product was estimated under visible light irradiation. Figs. 5(a-c) show the photocatalytic degradation of different

samples with different interval of time. It shows that the photocatalytic degradation performance of PbSe-G-TiO₂ nanocomposites are higher than that PbSe-G and TiO₂-G. During the passage of the time, the intensity of the characteristic absorption band of rhodamine B (555 nm) was significantly decreasing and after 180 min approximately 92.2 % of the organic dye was degraded. Moreover, kinetic of the degradation can be express as:

$$-\ln(C_t/C_0) = K_{\text{app}t} \quad (1)$$

$K_{\text{app}t}$ is apparent rate constant and C_0 initial concentration at $t = 0$ and C_t are the concentration of dye at $t = t$ [43]. The kinetic plot and apparent rate constant (K_{app}) (slop of the) in each case was shown in Fig. 5(d). It can be clearly seen that PbSe-G-TiO₂ ternary nanocomposite photo catalytic efficiency is almost 6 times higher than pure TiO₂. The recycling of catalysts is most important steps to estimate the practical application of photo-

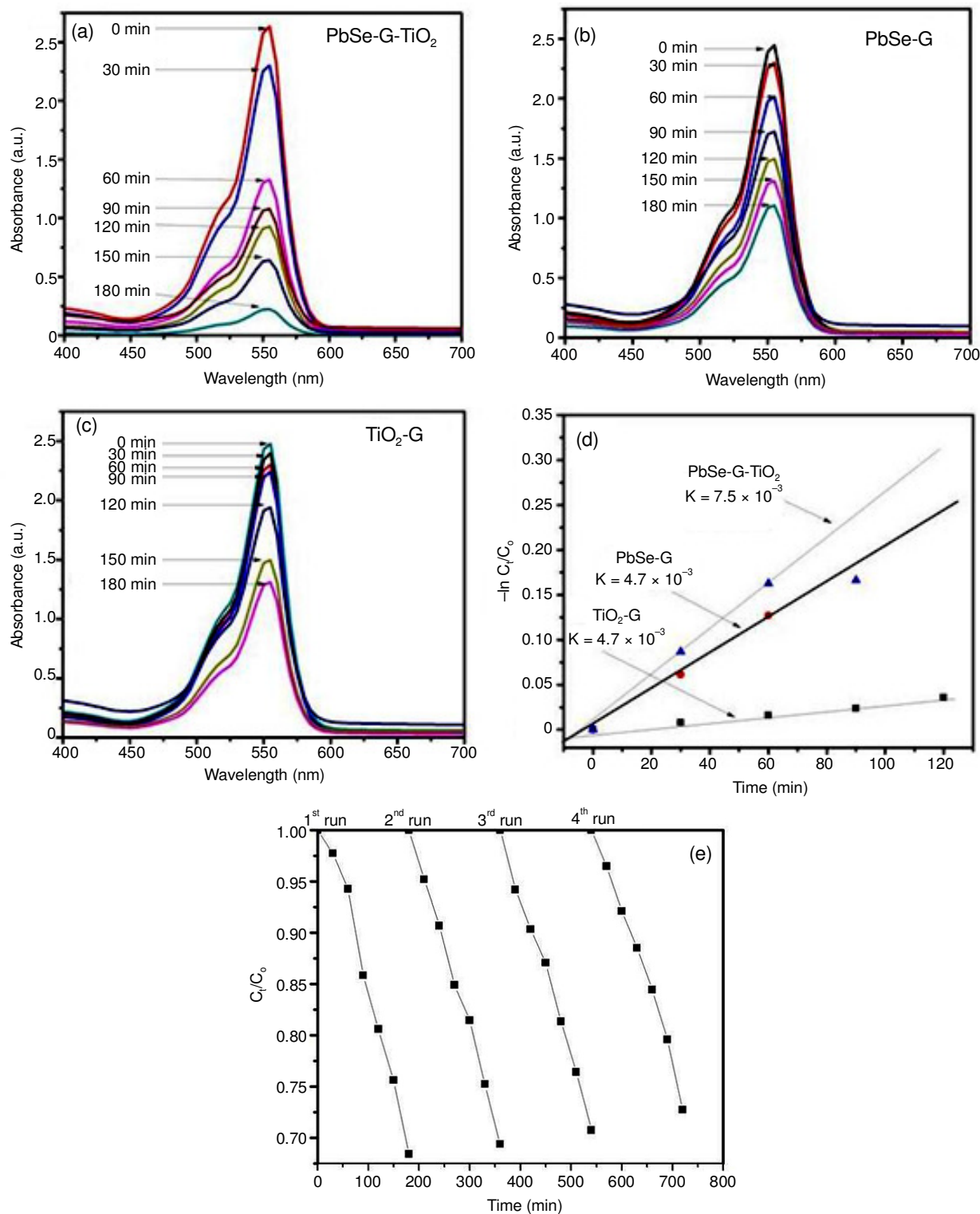


Fig. 5. Time-dependent absorption spectra of rhodamine B under visible light using (a) PbSe-G-TiO₂, (b) PbSe-G, (c) TiO₂-G, (d) kinetics of degradation of prepared composites under visible light irradiation and (e) recyclability of a PbSe-G-TiO₂ nanocomposite

catalysts. After four times recycling, it is clearly seen that the PbSe-G-TiO₂ nanocomposite did not show any significant loss of photocatalytic activity (Fig. 5e). Hence a PbSe-G-TiO₂ ternary nanocomposite shows great ability and therefore it is a promising candidate for environmental mediation.

Conclusion

In summary, PbSe-G-TiO₂ ternary nanocomposites were successfully synthesized by ultrasonic techniques for the photocatalytic degradation activity. Further PbSe-G-TiO₂ was characterized by XRD, SEM, TEM and RAMAN. The photocatalytic performance of PbSe-G-TiO₂, PbSe-G and TiO₂-G were evaluated using rhodamine B. It is clearly exhibited that PbSe-G-TiO₂ ternary nanocomposite can be used as a promising photocatalyst for the removing hydrophobic dyes. This work opens a new route to utilize graphene-based ternary nanocomposites for the energy and environmental-related applications.

REFERENCES

1. A. Khataee, M. Sheydaei, A. Hassani, M. Taseidifar and S. Karaca, *Ultrason. Sonochem.*, **22**, 404 (2015); <https://doi.org/10.1016/j.ultsonch.2014.07.002>.
2. J. Wang, T. Ma, Z. Zhang, X. Zhang, Y. Jiang, Z. Pan, F. Wen, P. Kang and P. Zhang, *Desalination*, **195**, 294 (2006); <https://doi.org/10.1016/j.desal.2005.12.007>.
3. N.J. Bejarano-Pérez and M.F. Suárez-Herrera, *Ultrason. Sonochem.*, **14**, 589 (2007); <https://doi.org/10.1016/j.ultsonch.2006.09.011>.
4. Z.-D. Meng and W.-C. Oh, *Ultrason. Sonochem.*, **18**, 757 (2011); <https://doi.org/10.1016/j.ultsonch.2010.10.008>.
5. R. Pelegrini, P. Peralta-Zamora, A.R. de Andrade, J. Reyes and N. Duran, *Appl. Catal. B*, **22**, 83 (1999); [https://doi.org/10.1016/S0926-3373\(99\)00037-5](https://doi.org/10.1016/S0926-3373(99)00037-5).
6. A. Konsowa, M. Ossman, Y. Chen and J.C. Crittenden, *J. Hazard. Mater.*, **176**, 181 (2010); <https://doi.org/10.1016/j.jhazmat.2009.11.010>.
7. S. Won, S. Choi, B. Chung, D. Park, J. Park and Y.-S. Yun, *Ind. Eng. Chem. Res.*, **43**, 7865 (2004); <https://doi.org/10.1021/ie049559o>.
8. Y.M. Slokar and A. Majcen Le Marechal, *Dyes Pigments*, **37**, 335 (1998); [https://doi.org/10.1016/S0143-7208\(97\)00075-2](https://doi.org/10.1016/S0143-7208(97)00075-2).
9. Y. Xu, R.E. Lebrun, P.-J. Gallo and P. Blond, *Sep. Sci. Technol.*, **34**, 2501 (1999); <https://doi.org/10.1081/SS-100100787>.
10. R. Ahmad, P.K. Mondal and S.Q. Usmani, *Bioresour. Technol.*, **101**, 3787 (2010); <https://doi.org/10.1016/j.biortech.2009.12.116>.
11. V. Gupta and Suhas, *J. Environ. Manage.*, **90**, 2313 (2009); <https://doi.org/10.1016/j.jenvman.2008.11.017>.
12. M.-S. Wu, T.-C. Wen and A. Gopalan, *Mater. Chem. Phys.*, **74**, 58 (2002); [https://doi.org/10.1016/S0254-0584\(01\)00406-0](https://doi.org/10.1016/S0254-0584(01)00406-0).
13. Y. Zhang, Q. Li, L. Sun, R. Tang and J. Zhai, *J. Hazard. Mater.*, **175**, 404 (2010); <https://doi.org/10.1016/j.jhazmat.2009.10.019>.
14. P. Lv, M. Zheng, X. Wang and F. Huang, *J. Alloys Comp.*, **583**, 285 (2014); <https://doi.org/10.1016/j.jallcom.2013.07.156>.
15. H.M. Yadav and J.-S. Kim, *J. Alloys Comp.*, **688**, 123 (2016); <https://doi.org/10.1016/j.jallcom.2016.07.133>.
16. Y. You, S. Zhang, L. Wan and D. Xu, *Appl. Surf. Sci.*, **258**, 3469 (2012); <https://doi.org/10.1016/j.apsusc.2011.11.099>.
17. F. Deng, Y. Li, X. Luo, L. Yang and X. Tu, *Colloids Surf. A*, **395**, 183 (2012); <https://doi.org/10.1016/j.colsurfa.2011.12.029>.
18. J. Yu, Q. Xiang and M. Zhou, *Appl. Catal. B*, **90**, 595 (2009); <https://doi.org/10.1016/j.apcatb.2009.04.021>.
19. G. Liu, M. Zhang, D. Zhang, J. Zhou, F. Meng and S. Ruan, *J. Alloys Comp.*, **616**, 155 (2014); <https://doi.org/10.1016/j.jallcom.2014.07.147>.
20. S. Bouhadoun, C. Guillard, F. Dapozze, S. Singh, D. Amans, J. Bouclé and N. Herlin-Boime, *Appl. Catal. B*, **174-175**, 367 (2015); <https://doi.org/10.1016/j.apcatb.2015.03.022>.
21. R. Asahi, T. Morikawa, T. Ohwaki, K. Aoki and Y. Taga, *Science*, **293**, 269 (2001); <https://doi.org/10.1126/science.1061051>.
22. Y.-C. Wu and L.-S. Ju, *J. Alloys Comp.*, **604**, 164 (2014); <https://doi.org/10.1016/j.jallcom.2014.03.023>.
23. J. Lei, Y. Chen, F. Shen, L. Wang, Y. Liu and J. Zhang, *J. Alloys Comp.*, **631**, 328 (2015); <https://doi.org/10.1016/j.jallcom.2015.01.080>.
24. M. Wang, L. Sun, Z. Lin, J. Cai, K. Xie and C. Lin, *Energy Environ. Sci.*, **6**, 1211 (2013); <https://doi.org/10.1039/c3ee24162a>.
25. L.-L. Tan, W.-J. Ong, S.-P. Chai and A.R. Mohamed, *Nanoscale Res. Lett.*, **8**, 465 (2013); <https://doi.org/10.1186/1556-276X-8-465>.
26. C. Stampfer, E. Schurtenberger, F. Molitor, J. Guttinger, T. Ihn and K. Ensslin, *Nano Lett.*, **8**, 2378 (2008); <https://doi.org/10.1021/nl801225h>.
27. K. Haubner, J. Murawski, P. Olk, L.M. Eng, C. Ziegler, B. Adolphi and E. Jaehne, *ChemPhysChem*, **11**, 2131 (2010); <https://doi.org/10.1002/cphc.201000132>.
28. F. Lupo, R. Kamalakaran, C. Scheu, N. Grobert and M. Rühle, *Carbon*, **42**, 1995 (2004); <https://doi.org/10.1016/j.carbon.2004.03.037>.
29. X.-Y. Zhang, H.-P. Li, X.-L. Cui and Y. Lin, *J. Mater. Chem.*, **20**, 2801 (2010); <https://doi.org/10.1039/b917240h>.
30. A.Z. Abdullah and P.Y. Ling, *J. Hazard. Mater.*, **173**, 159 (2010); <https://doi.org/10.1016/j.jhazmat.2009.08.060>.
31. K. Ullah, S. Ye, S.-B. Jo, L. Zhu, K.-Y. Cho and W.-C. Oh, *Ultrason. Sonochem.*, **21**, 1849 (2014); <https://doi.org/10.1016/j.ultsonch.2014.04.016>.
32. T. Ghosh and W. Oh, *J. Photocatal. Sci.*, **3**, 17 (2012).
33. M.A. Mahdy, I.A. Mahdy and E. Mahmoud, *Physica E*, **59**, 117 (2014); <https://doi.org/10.1016/j.physe.2014.01.009>.
34. L. Zhu, T. Ghosh, C.-Y. Park, Z.-D. Meng and W.-C. Oh, *Chin. J. Catal.*, **33**, 1276 (2012); [https://doi.org/10.1016/S1872-2067\(11\)60430-0](https://doi.org/10.1016/S1872-2067(11)60430-0).
35. S.D. Perera, R.G. Mariano, K. Vu, N. Nour, O. Seitz, Y. Chabal and K.J. Balkus Jr., *ACS Catal.*, **2**, 949 (2012); <https://doi.org/10.1021/cs200621c>.
36. L. Yoong, F.K. Chong and B.K. Dutta, *Energy*, **34**, 1652 (2009); <https://doi.org/10.1016/j.energy.2009.07.024>.
37. D. Li, M.B. Müller, S. Gilje, R.B. Kaner and G.G. Wallace, *Nat. Nanotechnol.*, **3**, 101 (2008); <https://doi.org/10.1038/nnano.2007.451>.
38. J.-J. Zhang, X. Liu, T. Ye, G.-P. Zheng, X.-C. Zheng, P. Liu and X.-X. Guan, *J. Alloys Comp.*, **698**, 819 (2017); <https://doi.org/10.1016/j.jallcom.2016.12.279>.
39. T. Tanaka, T. Sueishi, K. Saito, Q. Guo, M. Nishio, K.M. Yu and W. Walukiewicz, *J. Appl. Phys.*, **111**, 053522 (2012); <https://doi.org/10.1063/1.3691964>.
40. M. Ishii, K. Shibata and H. Nozaki, *J. Solid State Chem.*, **105**, 504 (1993); <https://doi.org/10.1006/jssc.1993.1242>.
41. P. Falaras, P. Papazafiri and P. Kitsiou, *Int. J. Nanomed.*, **9**, 3219 (2014).
42. R.-C. Wang, Y.-C. Chen, S.-J. Chen and Y.-M. Chang, *Carbon*, **70**, 215 (2014); <https://doi.org/10.1016/j.carbon.2013.12.110>.
43. J. Kyriakopoulos, M.D. Tzirakis, G.D. Panagiotou, M.N. Alberti, K.S. Triantafyllidis, S. Giannakaki, K. Bourikas, C. Kordulis, M. Orfanopoulos and A. Lycourghiotis, *Appl. Catal. B*, **117-118**, 36 (2012); <https://doi.org/10.1016/j.apcatb.2011.12.024>.